# Emergent Spatial Coordination from Negative Selection Alone: The Role of Observation Richness in Objective-Free Artificial Life

Anonymous

Abstract

We show that spatial coordination among agents emerges in a multi-agent grid world when agents can observe neighbor states, without any objective function guiding the search. Existing artificial life systems typically rely on fitness functions—explicit or implicit—which introduce evaluation bias and constrain the space of discoverable phenomena. We propose an objective-free approach based on large-scale random rule generation with viability-only filtering, comparing four observation conditions: random walk, a step-clock control, density-only observation, and state-profile observation. Across 5,000 rules per condition, agents with state-profile observation achieve nonzero median excess MI (MI calibrated by a permutation-based shuffle null that controls for pair-count bias) while density-only and control agents remain at zero (Cliff's $\delta = 0.355$; median-difference bootstrap 95% CI $[0.078, 0.111]$; Table 3), and the evidence ladder Control $\leq$ Phase 1 $<$ Phase 2 holds across all rule-based comparisons. A Miller-Madow bias-corrected estimator is used throughout, and a shuffle null confirms that the random walk's elevated raw MI is entirely attributable to pair-count bias ($\mathrm{MI}_{\mathrm{excess}}$ near zero at 0.050 bits, within the noise floor of the $N = 200$ shuffle null). Moran's $I$ further distinguishes local coordination from large-scale clustering. These results demonstrate that observation channel richness—not rule table capacity or selection pressure—drives the emergence of spatial coordination in objective-free systems.

Submission type: Full Paper

Data/Code available at: https://anonymous.4open.science/r/objectless-alife
Reproducibility map (artifact lineage): docs/reproducibility.md
PR26 follow-up archive DOI: https://doi.org/10.5281/zenodo.18713158

## Introduction

Artificial life research aims to understand the principles of living systems by constructing synthetic analogs (Bedau, 2003). A recurring challenge is the role of the objective function: most evolutionary and adaptive systems require an explicit fitness measure that guides search toward "interesting" configurations. Even novelty search (Lehman and Stanley, 2011), which abandons traditional fitness, still uses a novelty metric as an implicit objective.

This reliance on objectives introduces a subtle but pervasive bias. The choice of fitness function constrains which phenomena can emerge, and researchers may inadvertently encode their expectations into the evaluation criteria (Stanley et al., 2019). The question then arises: can meaningful spatial structure emerge in a multi-agent system with no fitness function?

We explore the unexplored quadrant of no objective $\times$ viability-only selection, where the only filtering criterion is physical consistency—removing rules that produce trivially broken simulations (all agents halt or converge to a single state). This viability-only filtering is analogous to the laws of physics: it constrains what is possible without specifying what is desirable. Importantly, this negative selection does constitute a minimal selection pressure (surviving rules must avoid degenerate dynamics), but no behavioral or performance criterion is employed.

Our core contribution is threefold:

1. A minimal grid-world model with objective-free negative selection, where random rule tables are evaluated and only physically inconsistent ones are discarded.

2. Evidence that observation richness—the amount of neighbor state information available to agents—drives emergent spatial coordination, independent of rule table capacity.

3. Robustness across four experimental conditions and 20,000 rule evaluations, with statistical significance confirmed by Mann-Whitney $U$ tests with Holm-Bonferroni correction.

## Related Work

Self-organization without selection. Cellular automata such as Conway's Game of Life (Gardner, 1970) and Wolfram's elementary rules (Wolfram, 1984) demonstrate that simple local rules can produce complex global patterns. Continuous extensions like Lenia (Chan, 2019) show rich morphogenetic dynamics in continuous state spaces. Reynolds' Boids (Reynolds, 1987) produce flocking behavior from three local rules. These systems share a common trait: the rules are hand-designed, not discovered through search.

Evolutionary ALife with fitness. Tierra (Ray, 1991) and Avida (Ofria and Wilke, 2004) use implicit fitness through resource competition and self-replication. While these systems produce open-ended dynamics, the replication criterion itself acts as a fitness function that selects for self-replicating programs.

Novelty search and open-endedness. Novelty search (Lehman and Stanley, 2011, 2008) replaces fitness with a novelty metric, enabling discovery of diverse behaviors. The open-ended evolution community has explored various approaches to sustaining innovation (Taylor et al., 2016; Stanley et al., 2019). However, all such approaches still employ an evaluation function—whether fitness, novelty, or complexity.

Information-theoretic measures. Mutual information and transfer entropy have been used to quantify coordination in multi-agent systems (Lizier et al., 2012). We use mutual information as a post-hoc analysis tool, never as a selection criterion.

Our position. Our approach differs from all the above by using no evaluation function —not fitness, not novelty, not complexity. We generate random rules, discard only physically broken ones, and ask what structure the surviving rules exhibit.

## Methods

### World Model

The simulation environment is a $20 \times 20$ toroidal grid populated by 30 agents (Figure 1). Each agent occupies exactly one cell (no overlap allowed) and maintains an internal state $s \in \{0, 1, 2, 3\}$. At each of 200 time steps, agents are updated in a random sequential order: one agent at a time observes its local neighborhood, looks up an action in a shared rule table, and executes it. The action space comprises 9 mutually exclusive actions: 4 cardinal movements, 4 state changes, and a no-op. Movement to an occupied cell fails silently.

Table 1: Model and experiment parameters.

| Parameter | Value |
|---|---|
| Grid topology | $20 \times 20$ torus (von Neumann) |
| Number of agents | 30 (7.5% density) |
| Internal states | $\{0, 1, 2, 3\}$ |
| Action space | 9 (4 moves, 4 state changes, 1 no-op) |
| Simulation steps | 200 |
| Update order | Random permutation each step |
| Halt window | 10 consecutive unchanged steps |
| MI estimator | Miller-Madow corrected, base-2 (bits) |
| Shuffle null $N$ | 200 permutations per rule |
| Seeds per condition | 5,000 (rule seed $i$, sim seed $i$) |

### Observation Phases

We compare four observation conditions that vary in the information available to agents:

Random Walk (RW). Each agent selects an action uniformly at random from $\{0, \ldots, 8\}$ at every step, ignoring the rule table entirely. This baseline isolates the contribution of grid geometry (collision avoidance, toroidal wrapping) from rule-driven behavior, and also serves to calibrate the MI estimator under conditions with minimal spatial clustering.

Control (step-clock). Agents observe their own state $s \in \{0, \ldots, 3\}$, the count of occupied von Neumann neighbors $n \in \{0, \ldots, 4\}$, and a periodic step clock $t \bmod 5 \in \{0, \ldots, 4\}$. The rule table has $4 \times 5 \times 5 = 100$ entries. The step clock provides no neighbor state information—it is a non-informative third dimension that matches the table size of Phase 2 without adding spatial content.

Phase 1: density-only (P1). Agents observe their own state $s$ and neighbor count $n$. The rule table has $4 \times 5 = 20$ entries, indexed by $5s + n$. This is the minimal observation that couples agents spatially.

Phase 2: state profile (P2). Agents observe their own state $s$, neighbor count $n$, and the dominant neighbor state $d \in \{0, \ldots, 4\}$ (the most frequent state among occupied neighbors, with ties broken by smallest value; 4 denotes no occupied neighbors). The rule table has $4 \times 5 \times 5 = 100$ entries, indexed by $25s + 5n + d$.


Figure 1: Grid snapshots of hand-picked highest-MI surviving rules from each condition (final-step grid; Miller-Madow estimator). MI values shown are for individual top-performing rules, not condition medians; see Table 2 for population statistics. Each panel shows the $20 \times 20$ toroidal grid with agents colored by internal state. Phase 2 rules produce visibly clustered spatial patterns, while Control rules appear disordered.

## Physical Filters

Only two filters are applied, both targeting physical inconsistency rather than behavioral quality:

- Halt detection: If all agents' positions and states remain unchanged for 10 consecutive steps, the simulation is terminated early.
- State uniformity: If all 30 agents converge to the same internal state, the simulation is terminated (an indistinguishable system is information-theoretically trivial).

No fitness function, novelty metric, complexity threshold, or behavioral criterion is used at any stage. Across 5,000 rules per condition, survival rates are: Random Walk 100%, Phase 1 71.4%, Phase 2 74.7%, Control 44.5%.

## Metrics

All metrics are computed post-hoc and never used for selection:

Neighbor mutual information (MI). For each pair of adjacent occupied cells $(i, j)$ on the toroidal grid, we compute the mutual information between their internal states:

$$I(S_i; S_j) = \sum_{s_i, s_j} p(s_i, s_j) \log_2 \frac{p(s_i, s_j)}{p(s_i)\, p(s_j)} \qquad (1)$$

where the joint and marginal distributions are estimated from all adjacent occupied pairs at a given time step. To mitigate the positive bias of the plug-in estimator at small sample sizes, we apply the Miller-Madow correction (Miller, 1955): $\hat{I}_{\mathrm{MM}} = \hat{I} - (K_{\mathrm{joint}} - K_X - K_Y + 1)/(2n \ln 2)$, where $K_{\mathrm{joint}}$, $K_X$, and $K_Y$ are the counts of non-zero bins in the joint and each marginal distribution respectively, and $n$ is the number of pairs. Values are clamped to $\geq 0$. High MI indicates that neighboring agents' states are statistically dependent—a signature of spatial coordination.

Shuffle-null MI calibration. To control for pair-count bias—where configurations with few neighbor pairs produce inflated MI estimates regardless of state structure—we compute a permutation-based shuffle null. For each rule's final snapshot, we fix occupied positions and randomly reassign states among them $N = 200$ times, computing $\hat{I}_{\mathrm{MM}}$ for each shuffle. Specifically, the shuffle operator preserves: (i) the set of occupied positions, (ii) the neighbor-pair graph structure, and (iii) the marginal state-frequency counts; it permutes only the assignment of states to positions. The mean across shuffles is the shuffle-null MI. The excess MI is then:

$$\mathrm{MI}_{\mathrm{excess}} = \max\big(\hat{I}_{\mathrm{MM}} - \overline{I}_{\mathrm{shuffle}},\ 0\big) \qquad (2)$$

which isolates genuine spatial coordination from estimation artifacts. All MI values are in bits (base-2 logarithm). In particular, the random walk's high raw MI ($\approx 0.91$ bits) is entirely attributable to pair-count bias: $\mathrm{MI}_{\mathrm{excess}}$ near zero (0.050 bits, within the noise floor of the $N = 200$ shuffle null).

Same-state adjacency fraction. Because agent states are categorical (nominal), traditional Moran's $I$ is inappropriate—it treats states as numeric, computing deviations from an arithmetic mean. We therefore report the same-state adjacency fraction (a join count statistic): the fraction of occupied neighbor pairs sharing the same internal state, bounded in $[0, 1]$. This is the standard spatial autocorrelation measure for categorical data.

Moran's I. Spatial autocorrelation is quantified by Moran's $I$ (Moran, 1950) across occupied cells using torus 4-neighborhood weights: both cells must be occupied for a weight of 1. Values range from $-1$ (dispersed) through 0 (random) to $+1$ (clustered). As noted above, Moran's $I$ treats states as numeric and is therefore a secondary indicator; the same-state adjacency fraction is the primary categorical spatial statistic.

State entropy. Shannon entropy (Cover and Thomas, 1991) of the internal state distribution across all agents: $H = -\sum_s p(s) \log_2 p(s)$.

Action entropy. Per-agent Shannon entropy of the cumulative action distribution, summarized as the mean and variance across agents.

## Experimental Design

For each of the four conditions, we generate 5,000 random rule tables using deterministic seeds (rule seeds 0–4,999, simulation seeds 0–4,999). Each rule table is evaluated on a single 200-step simulation. Surviving rules (those not terminated by halt or state-uniformity filters) have their final-step metrics recorded; all pairwise statistical comparisons use only surviving rules.

Statistical comparisons use two-sided Mann-Whitney $U$ tests (Mann and Whitney, 1947) with Holm-Bonferroni correction (Holm, 1979) applied across all metrics within each pairwise comparison. Each pairwise comparison (e.g., P1 vs. P2) tests a distinct hypothesis about the effect of observation content, so correction is applied per comparison rather than globally

across all stages. Effect sizes are reported as Cliff's $\delta$ (Cliff, 1993) (equivalent to rank-biserial correlation for Mann-Whitney $U$): $\delta = 1 - 2U_A/(n_1 n_2)$, where $U_A$ is the $U$ statistic for the first-listed group. To replace extreme $p$-values with more informative measures, we report bootstrap 95% confidence intervals (Efron, 1979) for the median difference (10,000 resamples, percentile method) as the primary effect-size statistic; $p$-values are retained as secondary evidence. Each rule table is paired with a single simulation seed (rule seed $i$ paired with simulation seed $i$), so per-rule conclusions reflect one initial configuration.

## Results

### Evidence Ladder Among Rule-Based Conditions

Table 2 and Figure 2 present the neighbor mutual information across all four conditions. Among the three rule-based conditions, a clear monotonic ordering emerges:

$$\text{Control} < \text{Phase 1} < \text{Phase 2}$$

The control condition, despite having 100-entry tables (equal to Phase 2), produces zero median excess MI—demonstrating that table size alone is insufficient. Phase 2 is the only rule-based condition with nonzero median excess MI, driven by access to neighbor state information (Table 3; bootstrap 95% CI excludes zero).

### Random Walk Baseline and Shuffle-Null Calibration

All MI values in this paper use the Miller-Madow bias-corrected estimator (Miller, 1955), which subtracts a first-order correction term from the naive plug-in estimate. However, this correction becomes insufficient when the number of neighbor pairs $n$ is comparable to the number of joint-distribution bins $K$—precisely the regime of random-walk agents, where ≈4–5 adjacent pairs populate up to 16 joint categories.

The shuffle null resolves this directly. By permuting states among fixed positions ($N = 200$ shuffles per rule), we obtain the expected MI under the null hypothesis of no spatial state structure. The excess MI ($\text{MI}_{\text{excess}} = \text{MI}_{\text{observed}} - \overline{\text{MI}}_{\text{shuffle}}$) isolates genuine coordination from pair-count artifacts.

For the random walk, $\text{MI}_{\text{excess}}$ is near zero (0.050 bits) (Table 2), confirming that its elevated raw MI is entirely attributable to pair-count bias—not spatial structure. In contrast, Phase 2 retains substantial excess MI, demonstrating genuine coordination that persists after bias calibration. Notably, the Control condition—not Phase 2—has the highest median Moran's $I$ (0.124), reflecting clustered but uncoordinated spatial patterns from its large table size. Phase 2's median Moran's $I$ ($-0.020$) is near zero, indicating that its elevated MI arises from local state coor-

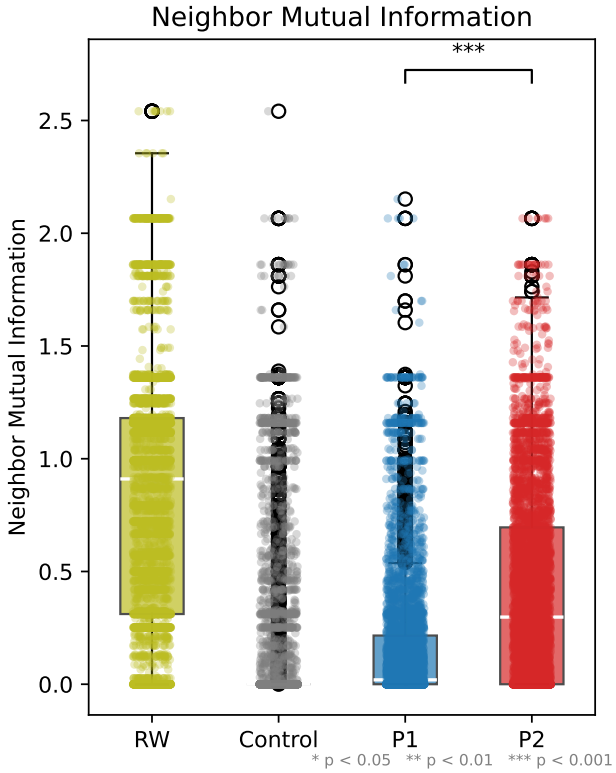


Figure 2: Final-step neighbor MI (Miller-Madow corrected, bits) distributions across rule-based conditions. Box plots with scatter strips show the full distribution for surviving rules. The evidence ladder Control < P1 < P2 is clearly visible.

Table 2: Calibrated neighbor mutual information and spatial clustering by condition. $\mathrm{MI}_{\mathrm{excess}} = \mathrm{MI}_{\mathrm{observed}} - \mathrm{MI}_{\mathrm{shuffle\ null}}$ is the primary calibrated metric controlling for pair-count bias (5,000 rules per condition, $N = 200$ shuffles). Raw MI values use the Miller-Madow bias-corrected estimator and are reported secondarily. The random walk's high raw MI is entirely attributable to pair-count bias ($\mathrm{MI}_{\mathrm{excess}}$ near zero at 0.050 bits, within the shuffle-null noise floor).

| Condition | Table Size | Median $\mathrm{MI}_{\mathrm{excess}}$ | Median MI | Median Adj. Frac.[1] | Survival |
|---|---|---|---|---|---|
| Random Walk | 1 (unused) | 0.050 | 0.910 | 0.364 | 100.0% |
| Control | 100 | 0.000 | 0.000 | 0.329 | 44.5% |
| Phase 1 | 20 | 0.000 | 0.019 | 0.291 | 71.4% |
| Phase 2 | 100 | 0.096 | 0.298 | 0.350 | 74.7% |

dination among neighbors rather than from large-scale spatial clustering.

The random-walk baseline remains informative: it validates the shuffle-null calibration procedure, establishes the bias floor, and confirms that all 5,000 random-walk rules survive (100% survival rate) since random actions never trigger halt or state-uniformity filters.

## Table-Size Confound Resolved

A natural objection is that Phase 2's higher MI could result from its larger rule table (100 entries vs. 20 for Phase 1), which permits more complex behaviors. The control condition resolves this confound directly: it uses 100-entry tables—identical in size to Phase 2—but replaces the informative dominant-neighbor-state dimension with a non-informative step clock. The control produces lower MI than Phase 1 despite having 5× more table entries. This demonstrates that observation content, not table capacity, drives emergent coordination.

The pairwise comparisons confirm this (Table 3): Phase 1 produces significantly higher MI than Control despite having smaller tables, and Phase 2 vastly exceeds Control despite equal table size.

## Filter-Selection Confound Check

A key methodological concern is that viability filters might indirectly favor high-MI rules, creating an apparent Phase 2 advantage through selection bias. To test this directly, we measured point-biserial correlation between survival status and final-step MI within each condition. The correlations are nearly identical for Phase 1 and Phase 2 ($r \approx 0.14$ in both), while Control is higher ($r = 0.45$) due to its substantially lower survival rate. The relevant comparison is therefore Phase 1 vs. Phase 2: because their filter–MI coupling is matched, the Phase 2 excess-MI advantage cannot be explained by differential filter selection.

## Temporal Dynamics

The four conditions exhibit qualitatively distinct temporal behaviors (Figure 3):

- Phase 1: MI rises quickly then plateaus—"frozen" dynamics where spatial patterns crystallize early.
- Phase 2: MI rises and remains dynamic, with ongoing fluctuations—sustained spatial coordination without freezing.
- Control: Highly chaotic trajectories with large MI variance and frequent collapses to zero.
- Random Walk: High but flat MI throughout, reflecting constant estimation bias from few adjacent pairs rather than genuine coordination.

This pattern is an exploratory qualitative observation only. It is consistent with a possible frozen–dynamic–chaotic ordering across conditions, but we do not claim edge-of-chaos evidence here because the analysis is based on a small sample of top-performing rules and does not include quantitative criticality measures (e.g., Lyapunov exponents).

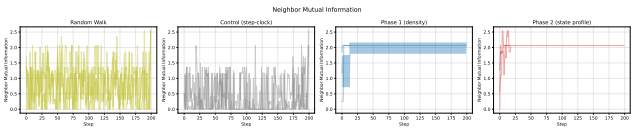


Figure 3: MI time-series trajectories for top-3 rules per condition. Phase 1 freezes early, Phase 2 remains dynamic, and Control shows chaotic fluctuations.

## Statistical Significance

Table 3 presents Mann-Whitney $U$ test results for the primary metric (neighbor MI) across all pairwise comparisons. All comparisons are highly significant after Holm-Bonferroni correction.

## Survival Analysis

Survival rates differ significantly across conditions (Table 2). Phase 2 achieves the highest survival rate, followed by Phase 1 and Control. State-uniformity is

Table 3: Pairwise statistical tests for $\mathrm{MI}_{\mathrm{excess}}$ (Eq. 2). Cliff's $\delta$ measures effect size (= rank-biserial $r$); bootstrap 95% CIs for the median difference (10,000 resamples) are the primary effect-size statistic; $p$-values (Holm-Bonferroni corrected) are secondary. Note that Cliff's $\delta$ measures stochastic dominance (probability that a random draw from one group exceeds the other), whereas the bootstrap CI estimates the location shift of the median difference.

| Comparison | Direction | $n_1$ | $n_2$ | Cliff's $\delta$ | Median diff 95% CI | $p$-value |
|---|---|---|---|---|---|---|
| P1 vs. P2 | P2 > P1 | 3570 | 3735 | 0.355 | [0.078, 0.111] | $< 10^{-252}$ |
| Ctrl vs. P1 | P1 > Ctrl | 2225 | 3570 | 0.124 | [< 0.001, < 0.001] | $< 10^{-50}$ |
| Ctrl vs. P2 | P2 > Ctrl | 2225 | 3735 | 0.423 | [0.078, 0.111] | $\approx 0$ |

the dominant termination mode for the control condition, suggesting that without neighbor state information, rules frequently drive all agents to the same state.

## Discussion

Observation richness as a driver of emergence. Our central finding is that the content of observation—specifically, access to neighbor state information—is the primary driver of emergent spatial coordination. This holds even when controlling for rule table size (the control condition). With shuffle-null-calibrated MI, Phase 2 is the only rule-based condition achieving nonzero median excess MI, while both Phase 1 and Control fall to zero—making the qualitative separation between observation conditions unambiguous. The same-state adjacency fraction (Table 2) provides a categorical spatial statistic appropriate for nominal state data. Phase 2's adjacency fraction (0.350) exceeds the random-placement expectation ($\approx 0.25$ for 4 equiprobable states), confirming local coordination. Moran's $I$ (reported in the supplementary material) is a secondary indicator, as it treats categorical states as numeric; nonetheless, it reveals that the Control condition exhibits the strongest spatial clustering (median $I = 0.124$) despite zero excess MI, while Phase 2's near-zero median $I$ ($-0.020$) indicates that its coordination operates at the local neighbor level rather than through large-scale spatial clustering. This result is not a consequence of having more rules to choose from, but of each rule being able to respond to richer local information.

Exploratory temporal pattern (not a primary claim). The temporal trajectories suggest a possible frozen–dynamic–chaotic ordering (Phase 1, Phase 2, Control), but we treat this strictly as exploratory context, not as evidence for edge-of-chaos theory. Establishing such a claim would require dedicated criticality analyses beyond the scope of the present work.

Viability filtering as minimal selection. Our methodology embodies a minimal philosophy: generate random configurations, remove only the physically broken ones, and examine what structure the survivors exhibit. We acknowledge that this "negative selection" constitutes a minimal selection pressure—surviving rules must avoid degenerate dynamics (halt or state uniformity)—but it is purely physical, imposing no behavioral or performance criterion. The surprising finding is that meaningful structure—quantified by mutual information—emerges even under this minimal regime, provided the observation channel is sufficiently rich.

Filter-metric independence. A potential concern is that viability filters might inadvertently select for high-MI rules, confounding the comparison between observation conditions. Point-biserial correlation between survival status and final-step MI yields $r = 0.14$ for Phase 2 ($p < 10^{-22}$), $r = 0.14$ for Phase 1, and $r = 0.45$ for Control. The Control's elevated correlation reflects its low survival rate (44.5% vs. ∼72% for rule-based conditions): stronger selection on survivors inflates the correlation mechanically. The relevant comparison is P1 and P2's near-identical $r \approx 0.14$, which indicates that the MI advantage of Phase 2 over Phase 1 is not an artifact of differential filter selection: both conditions have nearly identical filter-MI correlation, yet Phase 2 achieves substantially higher $\mathrm{MI}_{\mathrm{excess}}$.

Directional information flow. Transfer entropy analysis (supplementary material) confirms that the spatial coordination in Phase 2 involves genuine directional information flow from neighbor states to agent next-states, beyond what symmetric MI captures. This rules out the possibility that the observed MI arises from static correlations without dynamic coupling.

Capacity-matched controls. To further isolate the role of observation content from table capacity, we evaluated two additional control conditions (supplementary material): (i) a capacity-matched Phase 1 with 100-entry tables aliased to 20 effective observations, and (ii) a random-encoding Phase 2 with randomly permuted neighborhood-to-observation mappings. Both controls produce $\mathrm{MI}_{\mathrm{excess}}$ significantly below standard

Phase 2, confirming that structured encoding of neighbor state information—not table size or alphabet size—drives coordination.

Spatial scrambling confirmation. Spatial scrambling analysis (supplementary material) confirms that Phase 2's elevated MI depends on genuine local spatial coordination: randomly reassigning agent positions while preserving states reduces MI to near-zero levels, consistent with the shuffle-null calibration.

Role differentiation and temporal signatures. Beyond MI, our metric suite reveals additional dimensions of emergent structure (supplementary material, Section L). The variance of per-agent action entropy captures whether agents specialize into distinct behavioral roles: high variance indicates emergent role differentiation, where some agents consistently select the same action while others explore. Phase 2's access to dominant neighbor state is expected to support greater differentiation than Phase 1 or Control, where agents cannot distinguish neighbor identity. Quasi-periodicity peaks and phase-transition $\max \Delta$ provide temporal signatures that complement the MI time-series analysis: recurrent oscillatory patterns and abrupt reorganization events, respectively. Cross-condition differences in these temporal metrics further support the observation-richness narrative.

Filter cascade robustness. The main experiments apply only weak viability filters (halt detection, state uniformity). A cascaded filter analysis (supplementary material, Section M) applies additional medium-strength filters—short-period detection and low-activity detection—to test whether the Phase 2 MI advantage persists under stricter viability criteria. If the observation-richness ordering (Control $<$ P1 $<$ P2) holds among the more stringently filtered survivors, it strengthens the claim that coordination is a genuine property of the rule–observation interaction, not an artifact of lax filtering.

Implications for ALife research. These results suggest that objective-free search deserves more attention as a complement to fitness-driven approaches. When the goal is to discover what is possible rather than to optimize for a specific outcome, removing the objective function may reveal phenomena that fitness landscapes obscure. The key enabler is not the search algorithm but the architecture of the agents—specifically, what they can observe.

## Limitations

Several limitations constrain the generalizability of our findings:

- Single topology: All experiments use a $20 \times 20$ toroidal grid with von Neumann neighborhoods. Other topologies (hexagonal grids, Moore neighborhoods, irregular graphs) may produce different results.

- Symmetric metric: Mutual information is symmetric and measures correlation, not causation. Transfer entropy (supplementary material) confirms directional information flow in Phase 2, but a full time-resolved analysis remains for future work.

- No multi-generation evolution: Each rule table is evaluated in a single 200-step simulation. We do not evolve rules across generations, which limits comparison with evolutionary ALife systems.

- Small state space: With only 4 internal states and 9 actions, the model is deliberately minimal. Scaling to larger state spaces may reveal qualitatively different dynamics.

- Density fixed: The main experiments use 30 agents on a 400-cell grid (7.5% density). The supplementary material reports a systematic density sweep across 12 conditions (density range 0.017–0.400), confirming that the Phase 2 MI advantage holds across all tested densities.

- Sequential update order: Agents are updated in a random permutation each step, creating implicit temporal correlations between early and late updates within the same step. Synchronous update schemes may produce different dynamics.

- Single simulation per rule (main experiment): Each rule table is evaluated with a single initial configuration in the main experiment. The supplementary material provides multi-seed robustness analysis for the top 50 rules from each rule-based condition (Phase 2, Phase 1, and Control), confirming that MI levels—whether high, low, or zero—are stable properties of the rule table, not seed-specific accidents.

- Halt window sensitivity: The main experiments use a 10-step halt window. A sensitivity sweep across $\{5, 10, 20\}$ (supplementary material) confirms that results are robust to this parameter choice: survival rates and MI distributions remain qualitatively unchanged.

## Conclusion

We have shown that meaningful spatial coordination emerges in a multi-agent system through objective-free negative selection, and that the richness of agents' observation channels—not rule table capacity—is the critical factor. The evidence ladder from step-clock control through density-only to state-profile observation demonstrates a monotonic relationship between observation content and emergent coordination, confirmed by a bias-corrected MI estimator across all tested density levels (see the supplementary material).

Transfer entropy analysis (supplementary material) confirms directional information flow in Phase 2, and capacity-matched controls rule out table size as a confound. Future work should extend to larger grids and state spaces, explore multi-generation rule evolution under the same objective-free regime, and investigate whether richer observation channels enable qualitatively different forms of coordination. The broader implication is that the "remove broken, observe survivors" philosophy can serve as a productive complement to fitness-driven search in artificial life.

Supplementary Material. Density sweep analysis, multi-seed robustness results (all three rule-based conditions), halt-window sensitivity, survival rate confidence intervals, alternative null models, spatial scrambling analysis, transfer entropy, capacity-matched controls, algorithmic pseudocode, cross-condition metric profiles, and cascaded filter analysis are available as supplementary material with the code repository.

## References


Bedau, M. A. (2003). Artificial life: Organization, adaptation and complexity from the bottom up. Trends in Cognitive Sciences, 7(11):505–512.

Chan, B. W.-C. (2019). Lenia: Biology of artificial life. Complex Systems, 28(3):251–286.

Cliff, N. (1993). Dominance statistics: Ordinal analyses to answer ordinal questions. Psychological Bulletin, 114(3):494–509.

Cover, T. M. and Thomas, J. A. (1991). Elements of Information Theory. Wiley.

Efron, B. (1979). Bootstrap methods: Another look at the jackknife. The Annals of Statistics, 7(1):1–26.

Gardner, M. (1970). Mathematical games: The fantastic combinations of John Conway's new solitaire game "life". Scientific American, 223(4):120–123.

Holm, S. (1979). A simple sequentially rejective multiple test procedure. Scandinavian Journal of Statistics, 6(2):65–70.

Lehman, J. and Stanley, K. O. (2008). Exploiting open-endedness to solve problems through the search for novelty. In Proceedings of the Eleventh International Conference on Artificial Life (ALIFE XI), pages 329–336.

Lehman, J. and Stanley, K. O. (2011). Abandoning objectives: Evolution through the search for novelty alone. Evolutionary Computation, 19(2):189–223.

Lizier, J. T., Prokopenko, M., and Zomaya, A. Y. (2012). Local measures of information storage in complex distributed computation. Information Sciences, 208:39–54.

Mann, H. B. and Whitney, D. R. (1947). On a test of whether one of two random variables is stochastically larger than the other. The Annals of Mathematical Statistics, 18(1):50–60.

Miller, G. A. (1955). Note on the bias of information estimates. In Quastler, H., editor, Information Theory in Psychology: Problems and Methods, pages 95–100. Free Press, Glencoe, IL.

Moran, P. A. P. (1950). Notes on continuous stochastic phenomena. Biometrika, 37(1/2):17–23.

Ofria, C. and Wilke, C. O. (2004). Avida: A software platform for research in computational evolutionary biology. Artificial Life, 10(2):191–229.

Ray, T. S. (1991). An approach to the synthesis of life. In Langton, C. G., Taylor, C., Farmer, J. D., and Rasmussen, S., editors, Artificial Life II, pages 371–408. Addison-Wesley.

Reynolds, C. W. (1987). Flocks, herds and schools: A distributed behavioral model. In Proceedings of the 14th Annual Conference on Computer Graphics and Interactive Techniques (SIGGRAPH '87), pages 25–34. ACM.

Stanley, K. O., Lehman, J., and Soros, L. (2019). Why open-endedness matters. Artificial Life, 25(2):33–42.

Taylor, T., Bedau, M., Channon, A., Ackley, D., Banzhaf, W., Beslon, G., Dolson, E., Froese, T., Hickinbotham, S., Ikegami, T., McMullin, B., Packard, N., Rasmussen, S., Virgo, N., Agmon, E., Clark, E., McGregor, S., Ofria, C., Ropella, G., Spector, L., Stanley, K. O., Stanton, A., Timperley, C., Vostinar, A., and Wiser, M. (2016). Open-ended evolution: Perspectives from the OEE workshop in York. Artificial Life, 22(3):408–423.

Wolfram, S. (1984). Cellular automata as models of complexity. Nature, 311(5985):419–424.